Raman spectroscopy of thermally perturbed carbon fibers: Discriminating spectral responses of modulus classes and defect types

Z. E. Brubaker,* A. Miskowiec, and J. L. Niedziela†
National Security Sciences Directorate, Oak Ridge National Laboratory, Oak Ridge, Tennessee 37831, USA

(Received 8 February 2022; revised 24 May 2022; accepted 11 July 2022; published 21 July 2022)

The mechanical strength properties of carbon fibers are generally thought to be correlated with the presence of underlying atomic-level defects. These defects serve to break the underlying translational symmetry of the graphitic or graphene subunits of the fiber construction, resulting in the emergence of new Raman-active spectral features. However, historical attempts to classify the precise origin of defect contributions to the Raman spectra have been challenging because of indistinct and overlapping features in the carbon fiber Raman spectra. Further, while substantial research exists on high-temperature exposure in inert atmospheres for carbon fiber composites, comparatively less addresses microscale behaviors and Raman spectral alterations to monofilament carbon fibers exposed to high-temperature atmospheric environments. Here, we report Raman spectral responses of nine commercially available high-performance, polyacrylonitrile-based carbon fibers exposed to various atmospheric heat treatments. We introduce a model-independent characterization method, the integrated absolute difference, to quantify the spectral responses to heat treatment of different fiber modulus classes. We combine this new method with a newly reported strategy to standardize spectral fitting for carbon fibers. With this approach, we show that atomic-scale defects in the underlying fiber microstructure manifest in measurably distinct manners and have distinct responses to thermal perturbation. These combined approaches may lay the foundation for disentangling contributions from specific defects in the Raman spectra of carbon fibers.

DOI: 10.1103/PhysRevMaterials.6.073603

I. INTRODUCTION

Owing to their high strength-to-weight ratio, carbon fibers are increasingly used in high-performance applications, including aerospace design, transportation, and turbine blade manufacture for wind-energy generation [1,2]. With such substantial effects on the energy sector, the implications of having a thorough understanding of microscale changes to the structural integrity of carbon fibers are far reaching.

The manufacture of carbon fiber consists of polymerization, oxidation, carbonization, and graphitization steps, which have been described in detail elsewhere [1–3]. These manufacturing steps result in connected graphitic or graphene-like subunits interspersed with defects and voids that critically influence the carbon fiber mechanical properties [1,3]. The tensile properties are commonly clustered in terms of the bulk tensile moduli, with fibers having moduli between 200–280 considered standard modulus (SM), between 280–350 intermediate modulus (IM), and above 350 high modulus (HM). Minimization of the underlying defects in a material is generally thought to produce a higher performance fiber in terms of tensile strength, though higher graphitization produces more alignment of the graphitic plates, resulting in a reduced tensile strength and higher tensile modulus. Understanding how realistic and off-normal perturbations to the underlying crystal matrix of carbon fibers from thermal stress can contribute to the formation of defects is therefore of fundamental significance.

Raman spectroscopy is a powerful tool for characterizing carbon-based materials because the shapes, position, polarization, and relative amplitudes of the vibrational peaks reflect changes in the underlying graphitic structural units [4–6]. A great deal is thought to be known about how Raman spectral responses are altered in the presence of different kinds of defects [4–12], and failure mechanisms of composites at high temperature have been well studied [13–15]. However, comparatively less has been done to characterize the microscale behaviors and Raman spectral responses on individual fibers in the presence of high temperature in atmospheric environments, which could inform potential failure mechanisms of carbon fiber composites [16,17].

The first-order Raman spectra of carbon materials comprises the region between about 1100 and 1800 cm^{-1} and is surprisingly complex in spite of its apparent simplicity. The dominant peaks are located near 1350 and 1580 cm^{-1} and are known as the D1 and G peaks, respectively. The G band is related to the sp^2-bonded carbon atoms and is due to the doubly degenerate E_{2g} peak at the Brillouin zone center, whereas the D1 band is defect related, arising from a complex interaction with the electron band structure near the K point. Because of these coupling effects, the D1 band is dispersive in energy with incident laser excitation energy. Historically, the ratio of intensities of the D1 and G peaks has been used as a proxy for crystallite sizes [5–10,12,18–21], though absolute intensity determinations for Raman spectral investigations remain challenging [22].

*brubakerze@ornl.gov
†niedzielajl@ornl.gov

Additional peaks are occasionally reported in the 1100–1800 cm^{-1} region, including the D2 (or D′) peak near 1620 cm^{-1}, which arises from a mechanism similar to that of the D1 band, and the D3 (or A) and D4 (or I) peaks near 1500 and 1180 cm^{-1}, respectively. Multiple disparate models have been proposed to fit peaks for carbon fibers—preventing a uniform understanding—and individual spectral details are subject to variances in individual instrumental response functions. Poor characterization of these details continues to obfuscate the literature, but our recent work evaluating nearly 1000 Raman spectra across 32 commercially available carbon fibers demonstrated that standard-modulus (SM) and intermediate-modulus (IM) carbon fibers must be fitted with at least five peaks, and high-modulus (HM) fibers must be fitted with at least six peaks to establish any quantitative relationships [22].

In spite of the evident challenge in spectral fitting, a three-stage model has been proposed to correlate the Raman spectroscopic changes of carbon-bearing materials with the in-plane correlation length of the graphitic subunits [4,6]. For the present work, stages 1 and 2 are most pertinent: In stage 1, as the material becomes increasingly graphitic, (i) the G and D1 peaks sharpen, (ii) the D1 and G peaks move to lower wave numbers, and (iii) the relative intensity of the D1 and G bands (I_{D1}/I_G) decreases [4]. In stage 2, (i) the G (D1) peak moves to higher (lower) wave numbers, (ii) the G and D1 peaks sharpen, and (iii) I_{D1}/I_G increases as the degree of graphitization is improved. Thus, the Raman spectra of carbon-bearing materials can be correlated with microstructural defects, but achieving quantitative correlations hinges on consistent and robust fitting models.

Here, we use Raman spectroscopy to investigate the spectral evolution of high-performance polyacrylonitrile-based carbon fibers subjected to high-temperature perturbations in an atmospheric environment. We first evaluate the Raman spectra holistically by calculating the integrated absolute difference (IAD), which quantifies the Raman spectroscopic response of the thermally perturbed carbon fibers [23]. Then, we combine the results of the IAD analysis with traditional spectral fitting to develop an understanding of the microstructural changes that occur under these conditions and identify distinct Raman spectral responses for different fiber modulus classes. Finally, we demonstrate distinct combinations of Raman spectral parameters, which suggests that distinct defects manifest themselves in measurably distinct manners in the Raman spectra of carbon fibers.

II. MATERIALS AND METHODS

A. Fiber preparation

The investigated carbon fibers are summarized in Table I and span a broad range of tensile moduli and tensile strengths. All heat treatments were performed using a Linkam TS1500 temperature stage using 5–10 individual fibers per heat treatment. The length of the unperturbed fibers was less than 1 cm. For all treatments, the initial heating rate was 100 °C/min up to the maximum temperature, and the quench rate was nominally set to 200 °C/min, though below 550 °C radiative cooling is insufficient to retain this cooling rate, substantially slowing cooling. The fibers were held at either 375, 500, 580, 625, 680, 750, or 800 °C for 5 minutes; at treatments of 875 °C the fibers oxidized entirely, leaving no material behind.

TABLE I. Summary of the studied carbon fibers, including their tensile strength (TS) and tensile modulus (TM). All fibers are polyacrylonitrile-based and are sorted in order of increasing modulus. The values are as reported by the manufacturer and are not independently verified.

Fiber	Manufacturer	TS (GPa)	TM (GPa)
T700	Toray	4.90	230
AS4	Hexcel	4.41	231
T300	Cytec	3.65	231
IM7	Hexcel	5.65	276
T1000	Toray	6.37	294
IM10	Hexcel	6.96	310
M40	Toray	4.41	377
M46	Toray	4.21	436
HM63	Hexcel	4.69	441

B. Scanning electron microscopy

Scanning electron microscope (SEM) images were acquired using a Phenom XL desktop SEM with an excitation voltage of 5 or 10 kV. Fiber diameters were measured at five different locations along the fiber, and the reported uncertainty corresponds to one standard deviation of these values. Fiber diameters are included in the Supplemental Material [24].

C. Raman spectroscopy

Raman measurements were performed using a Renishaw inVia Raman microscope with a 100× objective using 532 nm lasers with the power held below 500 μW for all measurements. The laser spot size was approximately 1 μm. A grating of 2400 lines/mm with a spectral resolution of about 2.2 cm^{-1} was used. For all measurements, the incident polarization was parallel to the fiber axis, and the outgoing polarization was not controlled. The experimental configuration was such that only the fiber surface was probed; no measurements of fiber cross sections were collected. Measurements were collected on three to five spots for each fiber, and one to three fibers were measured for each heat treatment. In the case of the T700 fibers, heat treatments at 625 °C and 750 °C were repeated six times. All presented results correspond to the inverse-variance weighted average of either all spots for a given fiber or for all spots and fibers for a given thermal treatment. All uncertainties correspond to the standard deviation of the weighted mean, $\sigma = (\sum_i \sigma_i^{-2})^{-2}$. Raman spectra of SM and IM fibers were fitted using D1, D2, D3, D4, and G peaks, whereas the HM fibers were fitted using two D4 peaks, in addition to D1, D2, D3, and G peaks. The D1, D2, and G peaks were fitted using pseudo-Voigt line shapes, whereas all other peaks were fitted using Gaussian shapes. A complete discussion of the fitting model selection has been described previously [22]. As before, the L–G weighting parameter of the pseudo-Voigt function, n, is set to 1 (0) for pure Lorentzian (Gaussian) contributions. In cases where the peak positions reached the refinement bounds, these spectra and fits were discarded.

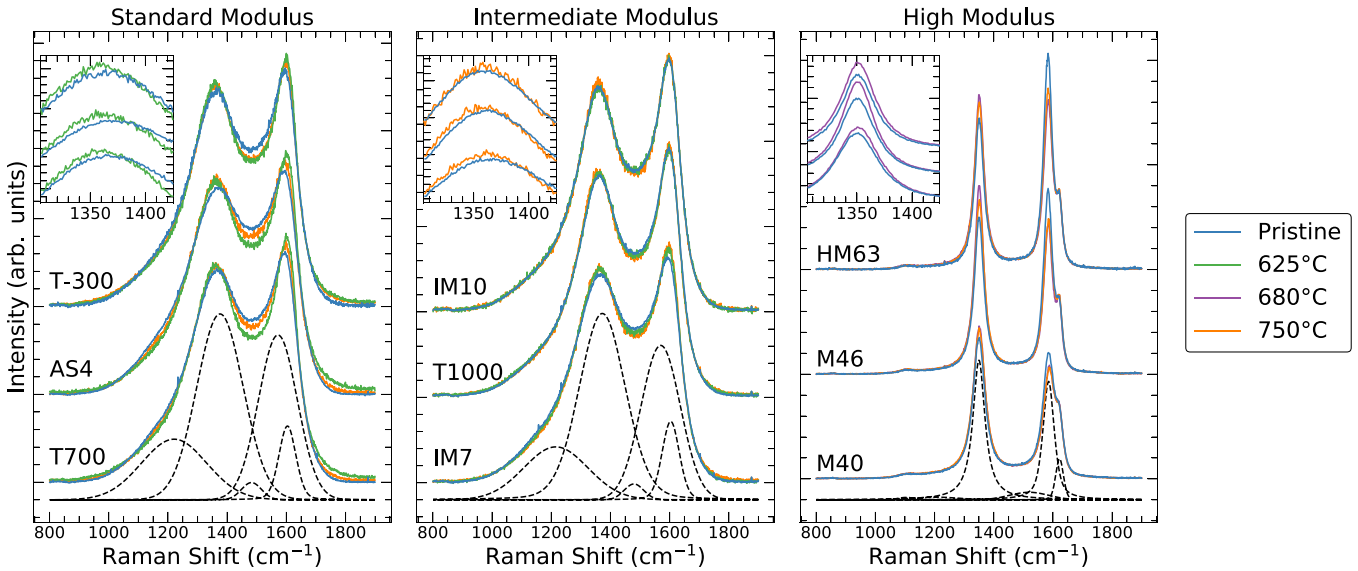

FIG. 1. Representative Raman spectra of heat-treated (a) SM, (b) IM, and (c) HM carbon fibers. All spectra are background subtracted and normalized to the total area. The SM fibers show the largest spectral response near 625 °C, whereas the HM fibers show the largest spectral response near 680 °C. The IM fibers show only subtle spectral changes, and the IM7 fibers—which are at the cusp between SM and IM fibers—show the largest spectral response of the IM fibers. The fit components of the unperturbed T700, IM7, and M40 spectra are shown with black dashed lines. Inset: Raman spectra focusing on the spectral region near the D1 peak, demonstrating subtle peak shifts observed for the SM, IM7, and M40 fibers. The order of the spectra is the same as the primary figure. For clarity, the reference spectrum is only compared to the spectrum of the heat-treated fiber yielding the largest spectral changes.

D. Integrated absolute difference

To quantify the degree of spectral change, we introduce the integrated absolute difference (IAD) concept. The IAD values are calculated by

$$\mathrm{IAD} = \int_{\mathrm{WN}_1}^{\mathrm{WN}_2} |s_{\mathrm{ref}} - s_{\mathrm{pert}}| d\mathrm{WN}, \tag{1}$$

where WN_1 and WN_2 are the first and last wave number of interest, s_{ref} is the spectrum of the pristine fiber, and s_{pert} is the spectrum of the perturbed fiber. We and others have applied similar calculations to x-ray emission spectroscopy experiments [23,25].

By calculating the IAD value, it is possible to quantify the magnitude of spectroscopic changes in the Raman spectra directly. Note, calculation of the IAD value requires the background to be subtracted and the data to be consistently normalized. To estimate the background, we fitted the spectra with a five-peak fitting model (six-peak fitting model) for SM and IM (HM) carbon fibers and estimated the background as linear. Similar backgrounds are achieved by linearly fitting the spectrum only below 900 and above 1800 cm^{-1}. Thus, the calculated IAD values are insensitive to the applied fit. After subtracting the background, we normalized to the total area of the spectrum. This normalization was chosen to avoid complicating effects of overlapping peaks and is consistent with work performed for x-ray emission spectroscopy measurements, though it may also be reasonable to normalize to other values. Finally, the region of integration was 800–1900 cm^{-1}.

III. RESULTS AND DISCUSSION

Figure 1 shows representative Raman spectra for each carbon fiber. All spectra show the typical D1 and G peaks expected for carbon fibers, and the D2 peak is clearly visible in the HM fibers. In the case of the SM fibers, ω_{D1} (ω_G) appears to decrease (increase) as a result of the thermal treatments. These peak shifts are consistent with an increasing degree of graphitization for materials in stage 2 of the three-stage model [4,6]. Interestingly, the strongest spectral response is observed near 625 °C rather than at the highest treatment temperatures. Near 625 °C, the tail of the G-spectral region extends to higher wave numbers, implying changing phonon lifetimes as the peak shape shifts from a Gaussian to a Lorentzian line shape.

In contrast, the intermediate modulus fibers show much weaker responses: the T1000 and IM10 fibers show hardly any spectral change, and the IM7 fibers (which lie at the cusp between SM and IM fibers) show gradual changes reminiscent of the standard modulus fibers. However, the IM7 fibers do not show the largest spectral response near 625 °C; rather, the spectral response increases gradually with increasing temperature.

For the HM fibers, the I_{D1}/I_G ratio increases after the heat treatments, but no peak shifts are observed. An increasing I_{D1}/I_G ratio implies a decreasing degree of graphitization for materials in stage 1 of the three-stage model and suggests that defects are being induced at the fiber surface. For thermally perturbed HM fibers, the largest spectral response is observed near 680 °C, a slightly larger temperature than that observed for the SM fibers.

To quantify the degree of spectral change, we calculate the IAD values for each heat treatment. Figure 2 shows the IAD

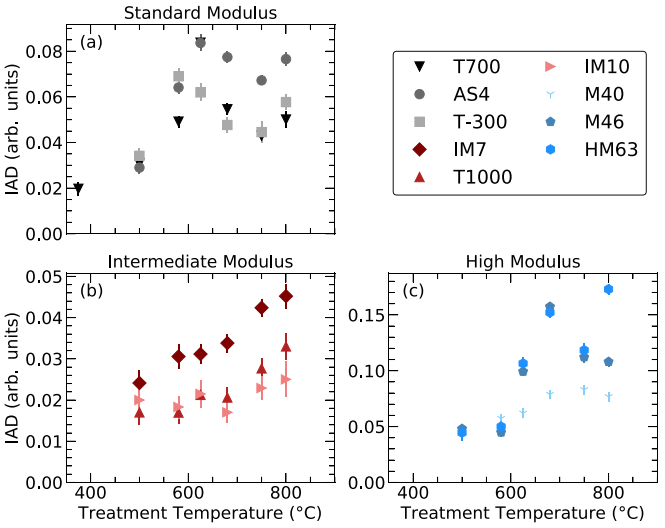

FIG. 2. Calculated IAD values as a function of treatment temperature for all carbon fibers. The SM fibers show a peak in spectral response near 580 and 625 °C, the IM fibers show a gradual increase in spectral response, and the HM fibers show a peak in spectral response near about 680 °C. The strongest spectral responses are observed for fibers with moduli most dissimilar to IM10 fibers, which we previously found to lie near the stage 1–stage 2 crossover [22].

values averaged across all spots and fibers for a given heat treatment; the Supplemental Material includes the IAD values prior to averaging across all fibers, revealing consistent spectral responses that justify averaging the IAD values [24]. The IAD values quantify the qualitative discussion above. The SM fibers show the largest spectral response near 580 and 625 °C, the IM7 fibers show a consistent, gradual change in Raman spectra, the T1000 and IM10 fibers show hardly any spectral change, and the HM fibers show a peak in spectral response near 680 °C. In the case of the SM and HM63 fibers, the IAD value appears to increase again above 750 °C, though this increase is not significantly larger than the uncertainties. In principle, it would be possible to use the IAD values—which are more reliably extracted than fit parameters—as a thermal probe, though the peak observed in the SM and HM fibers implies that a given IAD value could be achieved via multiple treatment temperatures. Importantly, this is not a shortcoming of calculating the IAD values, but rather a direct result of the Raman spectral response to thermal perturbations in oxidative conditions.

To understand whether the spectral response was the result of heat application alone or influenced by the atmosphere, we performed heat treatments of T700 fibers at 750 °C under vacuum; no spectral changes were observed. This result implies that the spectral response must be correlated with the oxidizing environment, so an oxidative mechanism occurs at the fiber surface. Critically, this mechanism must account for (i) a decreasing degree of graphitization in HM fibers, little or no change in the degree of graphitization in IM fibers, and an increasing degree of graphitization in SM fibers, and (ii) a peak in the spectral response as a function of treatment temperature.

We speculate that there exist two competing oxidative mechanisms. For the first mechanism, oxygen acts as a catalyst for subsequent reactions at the fiber surface. Carbon fibers undergo an initial stabilization step during manufacture, during which cyclization, dehydrogenation, and oxidation of the precursor polymer backbone are thought to occur [1,2]. This step is typically performed around 200–300 °C. Consequently, the higher-temperature treatments evaluated here result in a continuation of some of these reactions. We recently determined the relative hydrogen content of the T700, IM7, T1000, and IM10 fibers and found that lower modulus fibers contain the largest amount of hydrogen [26]. It is possible that standard modulus fibers are undergoing an oxygen-facilitated dehydrogenation process. This dehydrogenation process is thus comparatively inhibited in IM fibers because of the reduced hydrogen content natively present in the IM fibers after the oxidation process. On the other hand, oxygen-based defects are induced in HM fibers during the heat treatment, which results in a decreasing degree of graphitization at the fiber surface. The higher degree of graphitization of the HM fibers is achieved by higher carbonization temperatures during manufacture which drive off foreign elements, such as oxygen. Thus, the HM fibers may be more susceptible to inducing additional oxygen-based defects at reactive sites left vacant by the carbonization step. It is somewhat surprising that the IM fibers do not also show evidence of formation of additional oxygen-based defects, or significant response to the thermal perturbation. The resolution to this comes from the lack of residual hydrogen defects present after the oxidation step, and potential saturation of oxygen sites from the lower-temperature carbonization process.

The second oxidation mechanism occurs only at higher temperatures. In this mechanism, oxidation results in a full removal of the surface layer, exposing a fresh reactive surface promoting accelerated oxidation of the fiber. Thus, a peak in the spectral response and the measured IAD occurs when the speed of this mechanism becomes comparable to the first mechanism. This interpretation also implies that the largest spectral response should only be observed for heat treatment temperatures that minimally perturb the fiber diameter, which is, in fact, experimentally observed, and we explain this now. Figure 3 shows the IAD value as a function of relative fiber diameter at each thermal treatment temperature. For SM fibers, the largest IAD values occur between 580–680 °C. Beyond these temperatures the apparent diameter decreases, reflecting the crossover point between competing oxidation mechanisms. For the HM fibers, there is again a peak in the IAD response at 680 °C where the crossover point happens between oxygen inclusion and surface stripping mechanism. Above 680 °C, the fibers have all moved into a mode where the surface removal is operative, showing a uniform decrease in the fiber diameter as a function of heat treatment. Finally, at the highest thermal treatment temperatures, 800 °C (maroon pentagons), the largest shifts in relative fiber diameter are seen for all fibers, and they shift invariantly downward, corresponding to the end state removal of the surface layers dominated by the second oxidation mechanism. The IAD response for SM (average response 0.06) and HM fibers (average response 0.1) is larger than the response for the IM fibers (average IAD response 0.035). Additional information about the apparent

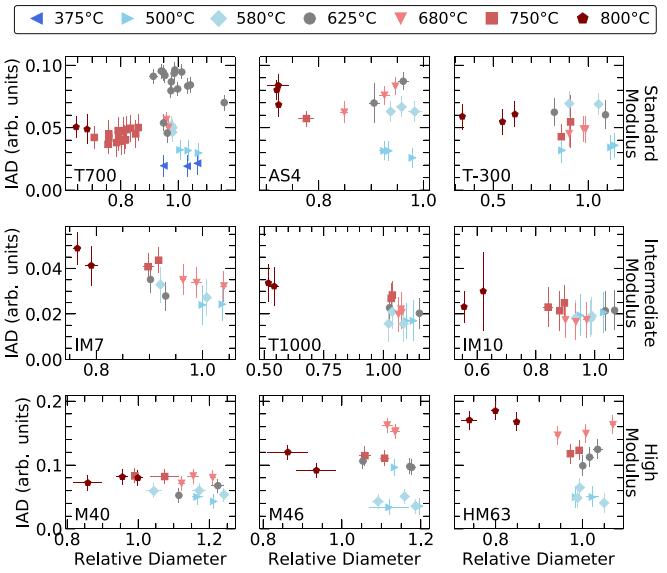

FIG. 3. IAD as a function of relative fiber diameter. In the case of the fibers that showed a peak in the spectral response near 600–680 °C (T700, AS4, T300, M46, and HM63 fibers), the largest IAD values are only observed near diameters of the pristine, unperturbed fibers. In the case of T300, M40, and M46 fibers, significant variations in fiber diameter were observed, which may result from striations that were observed along the fiber surface. The diameters are compared to the nominal diameter provided by the manufacturer.

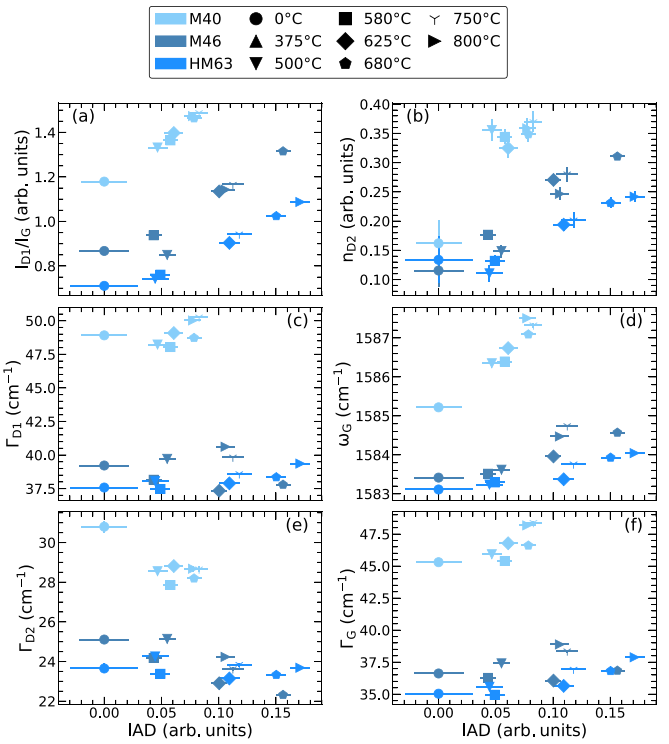

FIG. 4. Noteworthy fit parameters of the HM fibers as a function of IAD value. The fitting was performed as described previously [22]. The largest changes in Raman spectra are observed for ω_G, n_{D2}, and I_{D1}/I_G. The peak widths show comparatively smaller spectral changes. The spectral parameters are averaged for all spots and fibers for each thermal treatment. All remaining spectral parameters are included in the Supplemental Material [24].

fiber diameter as a function of heat treatment temperature is available in the Supplemental Material [24].

Now we have to address the fact that it is possible that as the surface layer is removed the Raman spectra are altered due to effectively varying probe depths. It is well established that the carbon fiber core is less graphitic than the fiber skin in SM fibers, whereas similar skin-core structures are generally not observed in IM and HM fibers [27–32]. High-resolution TEM measurements of T700 fibers suggest a core size of approximately 3.3 μm, with the core showing smaller crystallite sizes than the fiber skin [27,29]. These observations would suggest that we would expect to observe a decreasing degree of graphitization as the diameter is decreased. The few reports of Raman spectra across carbon fiber cross sections document the intensity or area ratios, which may show a minor increase near the fiber core, but these results are not significantly outside the reported uncertainties [33–35]. It is also important to note that the distinct incident polarization angle with respect to the carbon fiber basal planes for cross-sectional measurements as compared to the "top-down" geometry reported in the present work may alter the Raman spectra and complicate direct comparisons. Additionally, as we have previously pointed out, the intensity and area ratio are especially sensitive to the fitting model used [22].

Nonetheless, the available data suggest that varying probe depths cannot account for the observed spectral changes we ascribe to the dehydrogenation reaction: at temperatures below about 625 °C the diameter of the fibers remains relatively constant, and the spectral changes are far more substantial than any reports of Raman spectra across carbon fiber cross sections. On the other hand, it is possible that the spectral differences observed for the oxidative mechanism at temperatures beyond about 625 °C result from varying probe depths, but the current data make it challenging to conclusively ascertain the origin of these spectral changes. The fact that this mechanism only results in substantial spectral changes when the carbon fiber diameter is substantially reduced (see T1000 and IM10 fibers in Fig. 3) does hint at a probe-depth effect, but, contrarily, IM fibers like T1000 and IM7 have not shown evidence of a skin-core structure via HRTEM [32]. Further, in the case of the T700 fibers (and likely, all other SM fibers), the smallest fiber diameters observed after heat treatments remained larger than the reported core diameters [27], implying that the fibers never actually reach the core diameter. To definitively identify whether the probe depth is the origin of these spectral changes, it would be necessary to collect the Raman spectra of these fibers as a function of fiber diameter, which could be achieved by gradually polishing away surface layers of the carbon fibers.

Next, we evaluate the peak properties that contribute most strongly to the changing Raman spectra. We fit all spectra using the five-peak (D1, D2, D3, D4, G) fitting model for SM and IM carbon fibers, and the six-peak (D1, D2, D3, 2 × D4, G) for the HM fibers, as described previously [22]. Noteworthy spectral fit parameters are plotted as a function of IAD value for the HM fibers in Fig. 4 and for the SM and IM fibers in Fig. 5. The Supplemental Material includes all other

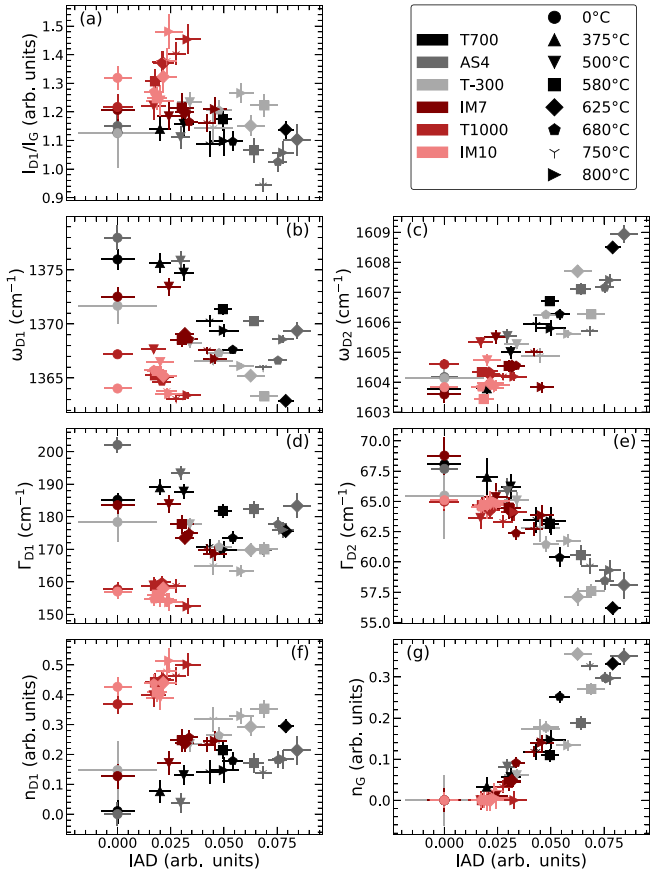

FIG. 5. Noteworthy fit parameters of the SM and IM fibers as a function of IAD value. The fitting was performed as described previously [22]. The T1000 and IM10 fibers show changes in ω_{D1} and I_{D1}/I_G. Conversely, the SM and IM7 fibers show significant changes in most D1, D2, and G fit parameters, with n_G, ω_{D1}, ω_{D2}, and Γ_{D2} showing the largest relative changes resulting from the thermal treatments. The spectral parameters are averaged for all spots and fibers for each thermal treatment. All other fit parameters are included in the Supplemental Material.

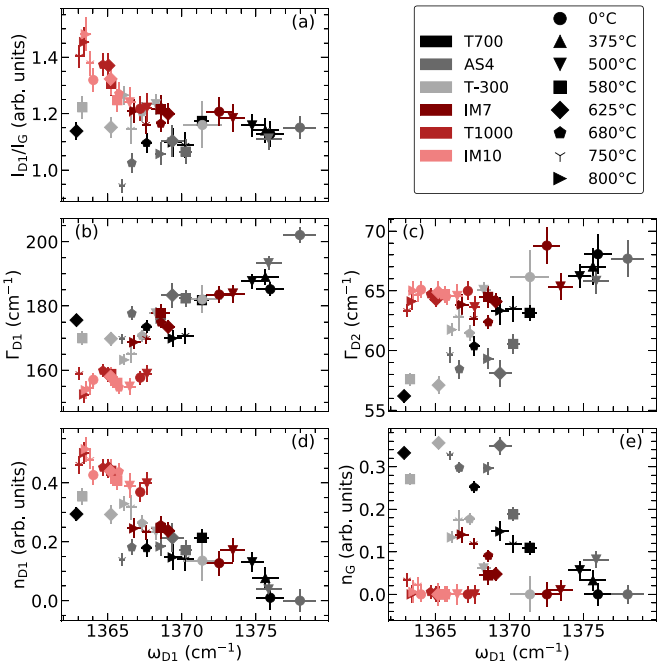

FIG. 6. Select spectral parameters of SM and IM fibers plotted as a function of ω_{D1}. At $\omega_{D1} < 1370$ cm^{-1}, significant differences between the SM and T1000 and IM10 fibers are observed. The most notable difference is n_G [panel (e)], demonstrating an increasing Lorentzian contribution to the G peak, which accounts for the high-wave-number tail observed in Fig. 1. Smaller differences are observed for other spectral parameters: Γ_{D1} is larger than the heat-treated SM fibers, whereas n_{D1}, I_{D1}/I_G, and Γ_{D2} are smaller for the heat-treated SM fibers. The remaining spectral parameters (not shown) only show minor or no distinctions.

spectral parameters, most of which which did not show any trends [24].

In the case of the HM fibers, the primary spectral changes are (i) an increase in I_{D1}/I_G, (ii) an increase in ω_G, and (iii) an increase in n_{D2}, implying an increasing Lorentzian line shape. The peak widths only show modest changes, with Γ_{D2} decreasing slightly, while Γ_G increases slightly. The increasing I_{D1}/I_G ratio implies a decreasing degree of graphitization in the three-stage model, consistent with our overall interpretation from the oxidation mechanisms described previously. The position of all D peaks remains largely consistent.

IM fibers T1000 and IM10 show only modest changes for most spectral parameters, but ω_{D1} decreases and I_{D1}/I_G increases. Because these fibers fall into stage 2 of the three-stage model, these spectral changes suggest that the degree of graphitization at the surface increases as a result of the thermal perturbations.

On the other hand, the SM and IM7 fibers show changes across many of the D1, D2, and G spectral parameters. The D1 peak position shifts by more than 10 cm^{-1} for the T700 and AS4 fibers, the D1 and D2 peaks narrow, and the G peak becomes increasingly Lorentzian. Further, the D2 peak shifts to higher positions and becomes increasingly Gaussian. These spectral changes imply an increasing degree of graphitization. Interestingly, the I_{D1}/I_G ratio remains largely unchanged for the SM and IM7 fibers unlike the T1000 and IM10 fibers that also fall in stage 2. Thus, not only does the magnitude of spectral response differ for each modulus class, but the spectral features contributing to the total change do as well.

For nuclear graphite, various defects manifest themselves in unique combinations of Raman spectral parameters [36]. The thermal perturbations of carbon fibers are expected to result in microstructural changes that differ from those introduced during manufacture. Importantly, our results yield overlapping ω_{D1} for all SM and IM fibers, which allows for similar analysis as performed for nuclear graphite. To that end, we plot a subset of the spectral parameters from Fig. 5 but transform the x axis to ω_{D1} as shown in Fig. 6.

Several fit parameters show clear distinctions between the SM and IM fibers in the range of overlapping ω_{D1}: Γ_{D1} (Γ_{D2}) are narrower (broader) for the T1000 and IM10 fibers, and I_{D1}/I_G is larger for T1000 and IM10 fibers. Most notably, however, is the Gaussian-Lorentzian weighting factor of the G peak, n_G: the G peak is entirely Gaussian for the T1000 and IM10 fibers but takes on an increasing Lorentzian shape in SM fibers. These results suggest that in the range of overlapping

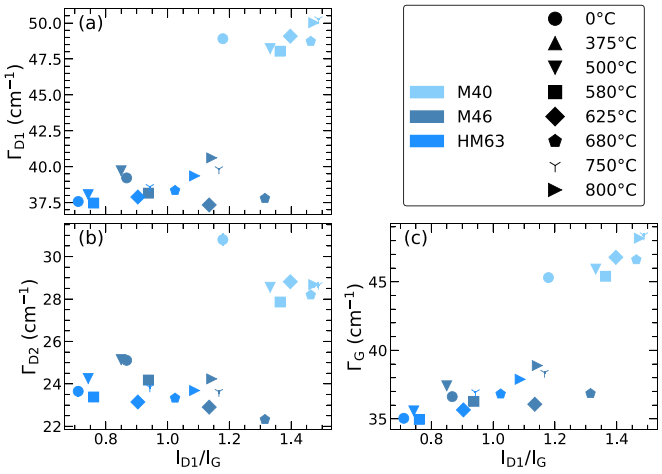

FIG. 7. Subset of the spectral parameters of the HM fibers plotted against the I_{D1}/I_G ratio. The peak widths, Γ_{D1}, Γ_{D2}, and Γ_G, show the largest separation between the M40 and other HM fibers. Similarly to the SM and IM fibers, these results imply that the combination of spectral parameters is nonunique, indicating that distinct defects manifest themselves in distinct manners.

ω_{D1} it is possible to classify fiber modulus class using only the Raman spectra of the thermally perturbed carbon fiber.

Similar differences in fit parameters can be obtained for the HM fibers by plotting the spectral parameters against the I_{D1}/I_G ratio (see Fig. 7). Here, the widths of the D1, D2, and G peaks allow for discrimination between the M46 and HM fibers—which possess very similar bulk moduli—and the M40 fibers, with a much lower bulk modulus. As in the case of the SM and IM fibers, these results suggest that the Raman spectra of the thermally perturbed fibers could be used to estimate the modulus of the pristine fiber.

Based on these differences in spectral parameters, Raman spectroscopy may be suitable for identifying—and, perhaps, even quantifying—specific defects contained in carbon fibers. For SM fibers, the magnitude of spectral changes may be correlated with the hydrogen content, whereas the spectral changes of the HM fibers likely arise from oxidation at the surface. If the role of these defects can be confirmed and quantified, it may be possible to disentangle the contributions of specific defects to the Raman spectra of carbon fibers. We previously identified broad correlations between the D1 Raman spectral parameters and mechanical properties, and we speculate that these relationships can be greatly improved if the contributions of specific defects can be disentangled [22].

IV. CONCLUSIONS

We have demonstrated that the Raman spectral response of SM, IM, and HM carbon fibers exposed to thermal perturbations differ substantially. By introducing the IAD concept, we are able to quantify the spectral response of the perturbed carbon fibers in a model-independent fashion, making it possible to use the IAD values as a thermal exposure probe.

Further, for each modulus class the total spectral change originates from distinct changes in peak widths, shapes, intensities, and line shapes. These differences arise from distinct contributions of specific defects contained in the carbon fiber matrix. Our results imply competing oxidative mechanisms, which may be consistent with (i) an oxygen-facilitated dehydrogenation process in SM fibers and (ii) the introduction of oxygen-based defects in the HM fibers. By comparing the specific combination of spectral fit parameters after heat treatments, we showcase the discriminatory power of Raman spectroscopy applied to thermally perturbed carbon fibers, and these results provide insight into the microstructural evolution of thermally perturbed carbon fibers of different modulus classes. Direct measurements of the oxygen content at the surface via x-ray photoemission spectroscopy could validate our proposed oxidative mechanism of the HM fibers.

ACKNOWLEDGMENTS

The authors thank S. Isbill and X. Zhou for a critical review of the document. This research was funded by the U.S. Department of Energy.

Z.E.B. conducted the experiment and analysis, A.M. contributed to data interpretation, and J.L.N. supervised the project. Z.E.B. wrote the manuscript with input from all authors.

[1] B. A. Newcomb, Composites, Part A **91**, 262 (2016).
[2] R. Böhm, M. Thieme, D. Wohlfahrt, D. S. Wolz, B. Richter, and H. Jäger, Fibers **6**, 56 (2018).
[3] D. D. Edie, Carbon **36**, 345 (1998).
[4] A. C. Ferrari and J. Robertson, Phys. Rev. B **64**, 075414 (2001).
[5] Y. Kaburagi, A. Yoshida, and Y. Hishiyama, *Materials Science and Engineering of Carbon—Characterization* (Elsevier, Amsterdam, 2016).
[6] A. C. Ferrari and J. Robertson, Phys. Rev. B **61**, 14095 (2000).
[7] G. A. Zickler, B. Smarsly, N. Gierlinger, H. Peterlik, and O. Paris, Carbon **44**, 3239 (2006).
[8] F. Tuinstra and J. L. Koenig, J. Chem. Phys. **53**, 1126 (1970).
[9] L. G. Cançado, K. Takai, T. Enoki, M. Endo, Y. A. Kim, H. Mizusaki, A. Jorio, L. N. Coelho, R. Magalhães-Paniago, and M. A. Pimenta, Appl. Phys. Lett. **88**, 163106 (2006).
[10] M. J. Matthews, M. A. Pimenta, G. Dresselhaus, M. S. Dresselhaus, and M. Endo, Phys. Rev. B **59**, R6585(R) (1999).
[11] P. Mallet-Ladeira, P. Puech, C. Toulouse, M. Cazayous, N. Ratel-Ramond, P. Weisbecker, G. L. Vignoles, and M. Monthioux, Carbon **80**, 629 (2014).
[12] D. S. Knight and W. B. White, J. Mater. Res. **4**, 385 (1989).
[13] G. Odegard and M. Kumosa, Compos. Sci. Technol. **60**, 2979 (2000).
[14] P. He, D. Jia, T. Lin, M. Wang, and Y. Zhou, Ceram. Int. **36**, 1447 (2010).
[15] F. Liu, B. Wu, and D. Wei, Fire Saf. J. **44**, 941 (2009).
[16] S.-M. Oh, S.-M. Lee, D.-S. Kang, and J.-S. Roh, Carbon Lett. **18**, 18 (2016).
[17] S. Feih and A. P. Mouritz, Composites, Part A **43**, 765 (2012).

[18] A. Cuesta, P. Dhamelincourt, J. Laureyns, A. Martínez-Alonso, and J. M. D. Tascón, J. Mater. Chem. **8**, 2875 (1998).
[19] O. A. Maslova, M. R. Ammar, G. Guimbretière, J.-N. Rouzaud, and P. Simon, Phys. Rev. B **86**, 134205 (2012).
[20] H. Okuda, R. J. Young, D. Wolverson, F. Tanaka, G. Yamamoto, and T. Okabe, Carbon **130**, 178 (2018).
[21] L. Nikiel and P. W. Jagodzinski, Carbon **31**, 1313 (1993).
[22] Z. E. Brubaker, J. J. Langford, R. J. Kapsimalis, and J. L. Niedziela, J. Mater. Sci. **56**, 15087 (2021).
[23] G. Vankó, T. Neisius, G. Molnár, F. Renz, S. Kárpáti, A. Shukla, and F. M. F. de Groof, J. Phys. Chem. B **110**, 11647 (2006).
[24] See Supplemental Material at http://link.aps.org/supplemental/10.1103/PhysRevMaterials.6.073603 for additional experimental and analytical details.
[25] Z. E. Brubaker, J. S. Harvey, J. R. Badger, R. R. Ullah, D. J. Campbell, Y. Xiao, P. Chow, C. Kenney-Benson, J. S. Smith, C. Reynolds, J. Paglione, R. J. Zieve, J. R. Jeffries, and V. Taufour, Phys. Rev. B **101**, 214408 (2020).
[26] Z. E. Brubaker, A. Miskowiec, Y. Q. Cheng, L. Daemen, and J. L. Niedziela, Phys. Rev. Materials **6**, 013609 (2022).
[27] G. Zhou, Y. Liu, L. He, Q. Guo, and H. Ye, Carbon **49**, 2883 (2011).
[28] L. Kong, H. Liu, W. Cao, and L. Xu, Fibers Polym. **15**, 2480 (2014).
[29] E. A. Morris, M. C. Weisenberger, M. G. Abdallah, F. Vautard, H. Grappe, S. Ozcan, F. L. Paulauskas, C. Eberle, D. Jackson, S. J. Mecham, and A. K. Naskar, Carbon **101**, 245 (2016).
[30] Y. Wang and T. H. Hahn, Compos. Sci. Technol. **67**, 92 (2007).
[31] B. A. Newcomb, L. A. Giannuzzi, K. M. Lyons, P. V. Gulgunje, K. Gupta, Y. Liu, M. Kamath, K. McDonald, J. Moon, B. Feng, G. P. Peterson, H. G. Chae, and S. Kumar, Carbon **93**, 502 (2015).
[32] R. Kulkarni and O. Ochoa, J. Compos. Mater. **40**, 733 (2006).
[33] X. Sui, Z. Xu, C. Hu, L. Chen, L. Liu, L. Kuang, M. Ma, L. Zhao, J. Li, and H. Deng, Compos. Sci. Technol. **130**, 46 (2016).
[34] H. Xiao, Y. Lu, M. Wang, X. Qin, W. Zhao, and J. Luan, Carbon **52**, 427 (2013).
[35] D. Li, C. Lu, G. Wu, Y. Yang, F. An, Z. Feng, and X. Li, RSC Adv. **4**, 60648 (2014).
[36] M. R. Ammar, N. Galy, J. N. Rouzaud, N. Toulhoat, C. E. Vaudey, P. Simon, and N. Monocoffre, Carbon **95**, 364 (2015).